FOCUS ISSUE OF SELECTED PRESENTATIONS FROM IMLB 2014

Dual Functions of Carbon in $Li_4Ti_5O_{12}$/C Microspheres

Lei Wen,[a] Zeyi Wu,[b] Hongze Luo,[c] Rensheng Song,[a] and Feng Li[a,z]

[a]*Shenyang National Laboratory for Materials Science, Institute of Metal Research, Chinese Academy of Sciences, Shenyang 110016, People's Republic of China*
[b]*Shenzhen Kingrunning Energy Materials Co., Ltd., Guanlan, Shenzhen 518000, People's Republic of China*
[c]*The Council for Scientific and Industrial Research, Pretoria 0001, South Africa*

Spinel $Li_4Ti_5O_{12}$ has become an alternative material to replace graphite anodes in terms of solving safety issues and improving battery life-time. Unfortunately, as $Li_4Ti_5O_{12}$ is an insulator, the low electrical conductivity becomes a major drawback, as it is unfavorable to higher rate capability. In addition to the low electronic conductivity, severe gassing during charge/discharge cycles is a critical but often-overlooked problem of $Li_4Ti_5O_{12}$ batteries. $Li_4Ti_5O_{12}$/C microspheres were prepared by assembling the nano-$Li_4Ti_5O_{12}$ (50–300 nm) with pitch derived pyrolytic carbon. It was found that the coated carbon in $Li_4Ti_5O_{12}$/C microspheres can effectively inhibit gassing and Mn deposition in $LiMn_2O_4$//$Li_4Ti_5O_{12}$ battery. Carbon can also significantly improve rate capability and cycling performance compared with that of $Li_4Ti_5O_{12}$ microspheres without carbon due to stable interface and superior electronic conductivity.

 [DOI: 10.1149/2.0061502jes]

Manuscript submitted October 20, 2014; revised manuscript received November 17, 2014. Published December 4, 2014. This was Paper 370 presented at the Como, Italy, Meeting of the IMLB, June 10–14, 2014. *This paper is part of the Focus Issue of Selected Presentations from IMLB 2014.*

Spinel lithium titanate ($Li_4Ti_5O_{12}$) has a high lithium intercalation voltage of 1.55 V vs. Lithium with a theoretical capacity of 170 $mAhg^{-1}$. $Li_4Ti_5O_{12}$ also has a high thermal stability, superior safety properties, and excellent cycle life. Since its discovery in the 1990s,[1] $Li_4Ti_5O_{12}$ has been investigated as a very promising alternative anode material, especially for large-scale batteries, such as hybrid electric vehicles (HEVs) or in renewable energy storage plants, due to its important properties including low cost, abundance, and environmental friendliness.[2]

Although it displays plenty of attractive characters, there are two main obstacles hindering application of $Li_4Ti_5O_{12}$. One is poor electronic and ionic conductivity, which leads to poor rate capability.[3,4] In addition, a number of strategies have been implemented to overcome the low electrical conductivity and to further improve the power performance of $Li_4Ti_5O_{12}$, including nanosized materials,[5–7] design of unique configurations,[8–11] carbon coating,[12–14] 3d-elements doping at Ti sites,[15–17] rare earth doping,[18] and coating with noble metal nano-particles, oxides or high conductive phase such as Ag[19], Cu_2O[20] and TiN phase,[3] which are expected to solve the challenge with good cyclic performance as well as to maintain a high rate performance.

Besides the low electronic conductivity, severe gassing during charge/discharge processes is a critical but often overlooked problem, particularly for $LiMn_2O_4$//$Li_4Ti_5O_{12}$ batteries. To date, this issue is unresolved, but it will clearly bear heavily on electrode materials, electrolyte, and battery system.[21–25] Recently, gassing in $LiNi_{1/3}Mn_{1/3}Co_{1/3}O_2$//$Li_4Ti_5O_{12}$ batteries has been attributed to the interfacial reactions between $Li_4Ti_5O_{12}$ and surrounding alkyl carbonate solvents by He and Kang et al.[23] Belharouak et al.[21] confirmed that gas generated in $LiMn_2O_4$//$Li_4Ti_5O_{12}$ systems during cycling is mainly composed of H_2, CO_2, and CO. It is suggested that H_2 is possibly derived from a trace of H_2O, while CO and CO_2 result from the decomposition of electrolyte solution initiated at relatively high temperatures by PF_5 that is a strong Lewis acid and one of the decomposition products of the electrolyte, $LiPF_6$.[21,23]

According to our results, gassing does not always occur. The most serious gassing only occurs when $LiMn_2O_4$ was used as the cathode. Less gassing is more likely when the cathode has high stability in electrolyte, such as $LiCoO_2$ cathode. Therefore, to further understand why gassing occurs and to find an effective way to control it, more investigation is needed for fabrication of $Li_4Ti_5O_{12}$ and reaction in $LiMn_2O_4$//$Li_4Ti_5O_{12}$ system.

We synthesized $Li_4Ti_5O_{12}$/C microspheres by assembling nano-$Li_4Ti_5O_{12}$ (50–300 nm) particles using pitch derived pyrolytic carbon. Coated carbon in $Li_4Ti_5O_{12}$/C played dual functions in $LiMn_2O_4$//$Li_4Ti_5O_{12}$ batteries. Carbon can effectively inhibit gas generation and Mn deposition in $LiMn_2O_4$//$Li_4Ti_5O_{12}$/C batteries, it also significantly improves rate capability and cycling performance compared with that of $Li_4Ti_5O_{12}$ microspheres without carbon due to stable interface and superior electronic conductivity.

Experimental

Materials synthesis.— Anatase TiO_2 (220 nm in average particle diameter and 99.5% in purity, Hangzhou Wanjing New Material Co., Ltd) and Li_2CO_3 (99.9% in purity, Shanghai China Lithium Industrial Co., Ltd.) were used as raw materials. The starting coarse $Li_4Ti_5O_{12}$ was prepared by a solid-state reaction method as described in a previous work.[26,27] The stoichiometric amounts of Li_2CO_3 and anatase TiO_2 with molar ratio of Li: Ti = 0.82:1 were mixed with ethanol as dispersant by planetary ballmilling. The ball-milled mixture was heated in a furnace at 800°C in air for 18 h to obtain the coarse $Li_4Ti_5O_{12}$.

Thereafter, $Li_4Ti_5O_{12}$ and $Li_4Ti_5O_{12}$/C microspheres were prepared by assembling nano-$Li_4Ti_5O_{12}$ particles with and without carbon. For the fabrication of $Li_4Ti_5O_{12}$ and $Li_4Ti_5O_{12}$/C microspheres, coarse $Li_4Ti_5O_{12}$ materials were first ball-milled without a carbon source and with 5 wt% pitch as a carbon source using water as a dispersant for 1.5 h, respectively. The resultant slurry was then spray dried to obtain the precursors individually. Finally, two precursors were all annealed at 650°C for 6 h in an Ar atmosphere to obtain the final materials.

Characterization.— X-ray diffraction (XRD) patterns of the samples were recorded on a Rigaku diffractometer using Cu Kα irradiation. Scanning electron microscopy (SEM) and transmission electron microscopy (TEM) images were obtained on a Nova NanoSEM 430 and Tecnai F20. Thermo gravimetric analysis (TGA, Netzsch-STA 449C) was used to analyze the carbon content in $Li_4Ti_5O_{12}$/C

[z]E-mail: fli@imr.ac.cn

at a heating rate of 10°C min^{-1} from 25 to 850°C in air. Raman spectra were obtained by a HORIBA Jobin Yvon LabRam HR800 micro-Raman spectroscope using 532 nm excited laser. X-Ray photoelectron spectroscopy (XPS) analysis was performed on the anodes of $LiMn_2O_4$//$Li_4Ti_5O_{12}$ and $LiMn_2O_4$//$Li_4Ti_5O_{12}$/C batteries after 10 cycles in order to identify the surface composition of the cycled electrodes. XPS images were taken with an ESCALAB 250 spectrometer using an AlKα radiation. Full batteries were disassembled in high-purity Ar atmosphere at 0% SOC (state of charge), rinsed thoroughly with dimethyl carbonate (DMC) solution, and then sealed in an air-tight container and transferred to the XPS apparatus with a minimal to air. To measure the tap density, 50 g powder was placed in a glass measuring cylinder, and tapped 100 times. The volume of the tapped powder and its mass was used to calculate the tap density.

Electrochemical characterizations of half cells.— Electrochemical characterization of $Li_4Ti_5O_{12}$ was carried out in CR2025 coin cells, using Li metal as the negative electrode, a Celgard 2400 polypropylene separators saturated with 1 M $LiPF_6$ in ethylene carbonate (EC), DMC and ethylene methyl carbonate (EMC), (1:1:1 w/w) as the electrolyte (Novolyte Technologies, Inc., Suchou, China). The electrode consisted of 90 wt% $Li_4Ti_5O_{12}$, 4 wt% polyvinylidene fluoride (PVDF) as a binder, and 6 wt% acetylene black. These materials were dispersed in 1-methyl-2-pyrrolidinone (NMP), and the resultant slurry was then coated onto an aluminum foil. Typically, ∼7 mg of the mixed powders was used per cell. Charge/discharge tests were conducted at room temperature using a LAND CT2001A tester at various current densities from 0.2 to 20 C between 2.7 and 0.8 V (1 C = 175 mAh/g). AC impedance spectra were measured by a Solatron 1260 Impedance Analyzer in the frequency range from 10 mHz to 100 kHz with a potential perturbation at 10 mV.

Assembly of $LiMn_2O_4$//$Li_4Ti_5O_{12}$ batteries.— The 043048-type pouch cells were assembled using $Li_4Ti_5O_{12}$ and $Li_4Ti_5O_{12}$/C anode electrodes with $LiMn_2O_4$ (Hunan Shanshan Toda Advanced Materials Co., Ltd) cathode electrodes. The $LiMn_2O_4$ electrode consisted of 95 wt% $LiMn_2O_4$, 2 wt% conductive carbon black, and 3 wt% PVDF. The $Li_4Ti_5O_{12}$ and $Li_4Ti_5O_{12}$/C electrode consisted of 92 wt% active materials, 3 wt% conductive carbon black, and 5 wt% PVDF as binder. 1M $LiPF_6$ in a 1:1:1 mixture of EC/DMC/EMC was used as the electrolyte and Celgard 2400 polypropylene separator was used as separator. The cathode electrode, anode electrode, and separator were wound together to make the battery core, and then the core was put into a 043048-type aluminum plastic-laminated film box. The electrolyte was injected and the batteries were sealed with a sealing machine. The cell assembly was conducted in an argon-filled glove box. Cyclic voltammograms were recorded by a Solartron 1287 electrochemical workstation. Charge/discharge tests were conducted at room temperature using a LAND CT2001B tester at 1C (1C=290mA).

Results and Discussion

Morphology and structural characterization.— Due to the carbon coating, tap density of $Li_4Ti_5O_{12}$/C materials was about 1.05 g/cm^3, which is lower than that of pure $Li_4Ti_5O_{12}$ materials (1.20 g/cm^3). Figure 1 shows the XRD patterns of (a) $Li_4Ti_5O_{12}$/C and (b) $Li_4Ti_5O_{12}$. All the diffraction peaks at 2θ of 18.4, 35.6, 43.3, 47.4, 57.2, 62.8, and 66.1, in both XRD patterns can be indexed as spinel $Li_4Ti_5O_{12}$ according to the JCPDS powder diffraction file No. 49–0267 and no impurity peaks were detected. These results indicate that pyrolytic carbon has no effect on the crystal structure of spinel $Li_4Ti_5O_{12}$. The percentage of carbon in $Li_4Ti_5O_{12}$/C was about 2.6 wt% based on the TGA. Weight loss is due to thermal decomposition of pitch at high temperatures. Raman spectroscopy was used to characterize $Li_4Ti_5O_{12}$ and $Li_4Ti_5O_{12}$/C. As shown in Fig. 2, besides Raman peaks of $Li_4Ti_5O_{12}$ at 230, 350, 422, and 670 cm^{-1} in Fig. 2b, the D-band around 1326 cm^{-1} and G-band around 1590 cm^{-1} can be clearly seen in Raman spectra of the $Li_4Ti_5O_{12}$/C (Fig. 2a), which are the characterization peaks of carbon materials.

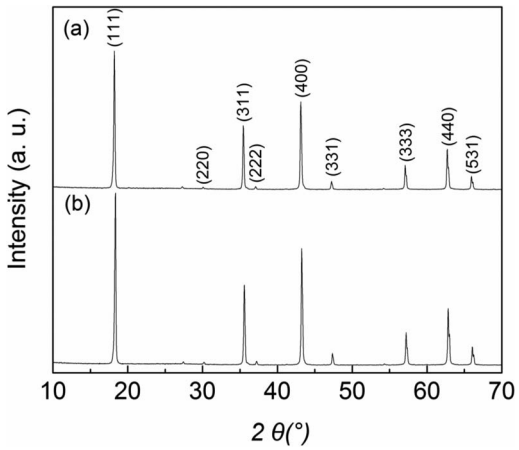

Figure 1. XRD patterns of (a) $Li_4Ti_5O_{12}$/C and (b) $Li_4Ti_5O_{12}$.

The difference of surface morphology between $Li_4Ti_5O_{12}$ and $Li_4Ti_5O_{12}$/C can be observed in Fig. 3. Both materials are spherical, with a size of ∼20–50μm. As shown in Fig. 3a and 3b, the agglomerates of particles located in the $Li_4Ti_5O_{12}$ spheres cause rough surfaces and porous structure of $Li_4Ti_5O_{12}$. While for $Li_4Ti_5O_{12}$/C, it has smooth surface and uniform structure (Fig. 3c and 3d). Figure 3e and 3f show TEM morphologies of $Li_4Ti_5O_{12}$/C, its primary particle size is ∼50–300nm, and the thickness of carbon layer is ∼10–30 nm.

Electrochemical performances in half-cells.— Figures 4a and 4b show the charge and discharge curves of $Li_4Ti_5O_{12}$ and $Li_4Ti_5O_{12}$/C, respectively. Note that the $Li_4Ti_5O_{12}$ shows high specific capacity ∼167 mAh/g at 0.2C, 159 mAh/g at 1 C. At higher charge/discharge rates, such as 5 C, 10 C, and 20 C, it shows much lower specific capacity of 136, 118, and 92 mAh/g, respectively. In Fig. 4b, we can clearly see that $Li_4Ti_5O_{12}$/C shows superior charge/discharge performance at high rates. It delivers 171, 165, 145, 131, and 110 mAh/g at 0.2, 1, 5, 10, and 20 C rates,respectively. Figure 4c compares the polarization between the charge and discharge plateau for the two electrodes shown in Fig. 4a and 4b. This potential difference can represent the degree of polarization of the electrode. Polarization for the $Li_4Ti_5O_{12}$/C electrode are much smaller than those of $Li_4Ti_5O_{12}$ electrode at all discharge rates from 1 C to 20 C, which again shows that the $Li_4Ti_5O_{12}$/C has better reaction kinetics, because of the improved electrical conductivity by carbon coating. The trends in the capacity change were found to correlate well with the charge-transfer resistance determined by electrochemical impedance spectra (EIS)

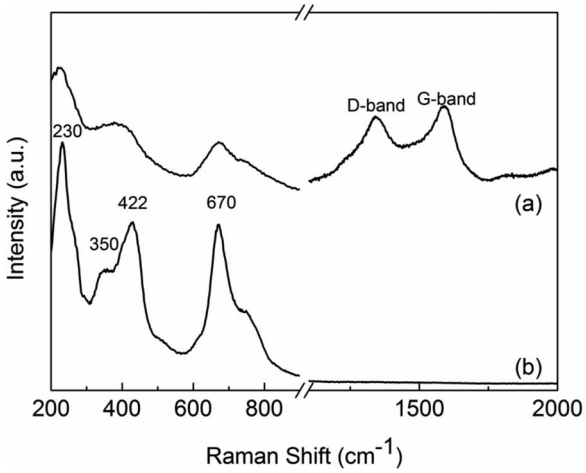

Figure 2. Raman spectra of (a) $Li_4Ti_5O_{12}$/C and (b) $Li_4Ti_5O_{12}$.

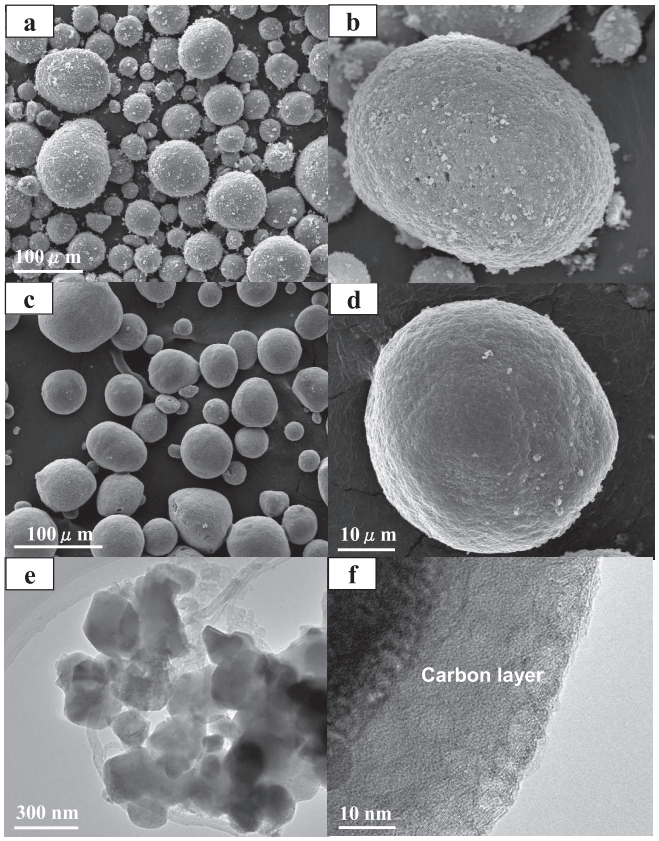

Figure 3. SEM images of $Li_4Ti_5O_{12}$ (a and b), and $Li_4Ti_5O_{12}$/C (c and d), TEM images of $Li_4Ti_5O_{12}$/C (e and f).

analysis.The Nyquist plots shown in Fig. 4d show a prominent semi-circle within the high-frequency range. The width of this semi-circle gives the approximate overall charge transfer resistance (R_{ct}).[28] It was found that the $Li_4Ti_5O_{12}$/C has a lower R_{ct} (~27.5 Ω) than that of $Li_4Ti_5O_{12}$ (~51.5 Ω). Due to similar experimental conditions, such as loading of the $Li_4Ti_5O_{12}$ (6.2 ± 0.1 mg/cm^2) and test temperatures, the observed difference in the charge-transfer resistance is apparently due to ionic and electronic conductivities of two samples.

Role of carbon for suppressing gassing.— The electrochemical performance of $Li_4Ti_5O_{12}$ and $Li_4Ti_5O_{12}$/C was further evaluated using pouch batteries. Figures 5a and 5b show the charge-discharge curves of $LiMn_2O_4$//$Li_4Ti_5O_{12}$ and $LiMn_2O_4$//$Li_4Ti_5O_{12}$/C batteries at 1 C, respectively. Obviously, $LiMn_2O_4$//$Li_4Ti_5O_{12}$/C has a superior rate performance to that of $LiMn_2O_4$//$Li_4Ti_5O_{12}$. For example, in the tenth cycle, the discharge capacity, galvanostatic capacity proportion, and average discharge plateau are 281 mAh, 88.5% and 2.42 V for $LiMn_2O_4$//$Li_4Ti_5O_{12}$ batteries, and 289 mAh, 96.2% and 2.46 V for $LiMn_2O_4$//$Li_4Ti_5O_{12}$/C batteries, respectively. This is mainly because carbon coating leads to the increase of electronic conductivity and enhanced electrochemical performance. The $LiMn_2O_4$//$Li_4Ti_5O_{12}$/C batteries also show superior cycle performance to that of $LiMn_2O_4$//$Li_4Ti_5O_{12}$ battery (Fig. 5b). The capacity retention proportion of $LiMn_2O_4$//$Li_4Ti_5O_{12}$ batteries is only 23% at the 580th cycles. In contrast, the capacity retention proportion of $LiMn_2O_4$//$Li_4Ti_5O_{12}$/C batteries is 93% even at the 1000th cycle.

More importantly, it is noted from the inset of Fig. 5b that the swelling obviously occurred for $LiMn_2O_4$//$Li_4Ti_5O_{12}$ batteries by generated gas after long cycling. However, no swelling can be observed for the $Li_4Ti_5O_{12}$/C based battery even after 1000 cycling. This indicates that carbon can suppress gassing effectively.

Cyclic voltammograms (CV) of the two batteries was conducted to study the function of carbon for suppressing gassing, as shown in Fig. 6. These cells had similar loadings of LTO and LTO/C materials. The peaks at 2.6 and 2.7 V during the first positive scan and the peaks at 2.3 and 2.4 V during the first negative scan presents a typical electrochemical characteristic attributed to the two steps of reversible

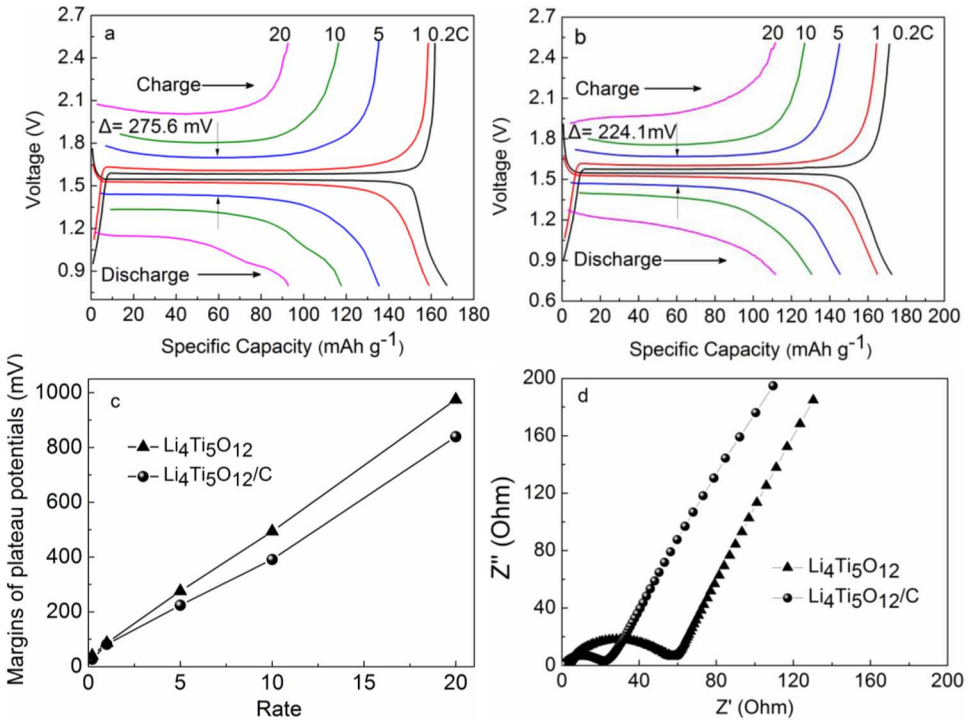

Figure 4. Charge and discharge curves of (a) $Li_4Ti_5O_{12}$ and (b) $Li_4Ti_5O_{12}$/C electrodes from 0.2 C to 20 C, (c) Comparison of the charge and discharge plateau potential difference, (d) EIS of $Li_4Ti_5O_{12}$ and $Li_4Ti_5O_{12}$/C.

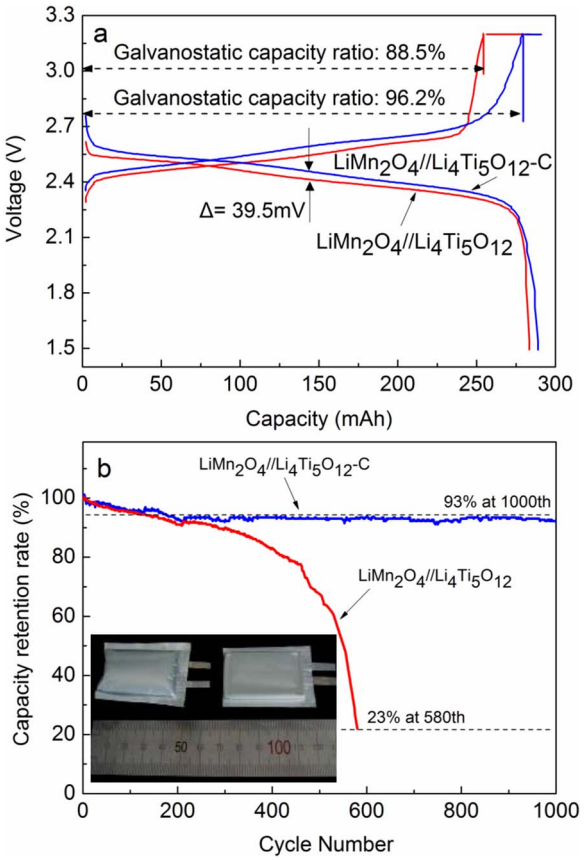

Figure 5. (a) Charge-discharge curves of $LiMn_2O_4//Li_4Ti_5O_{12}$ and $LiMn_2O_4//Li_4Ti_5O_{12}$/C batteries at 10th cycle, (b) Cycling performance of $LiMn_2O_4//Li_4Ti_5O_{12}$ and $LiMn_2O_4//Li_4Ti_5O_{12}$/C batteries, the inset is a photograph of $LiMn_2O_4//Li_4Ti_5O_{12}$ and $LiMn_2O_4//Li_4Ti_5O_{12}$/C batteries, respectively.

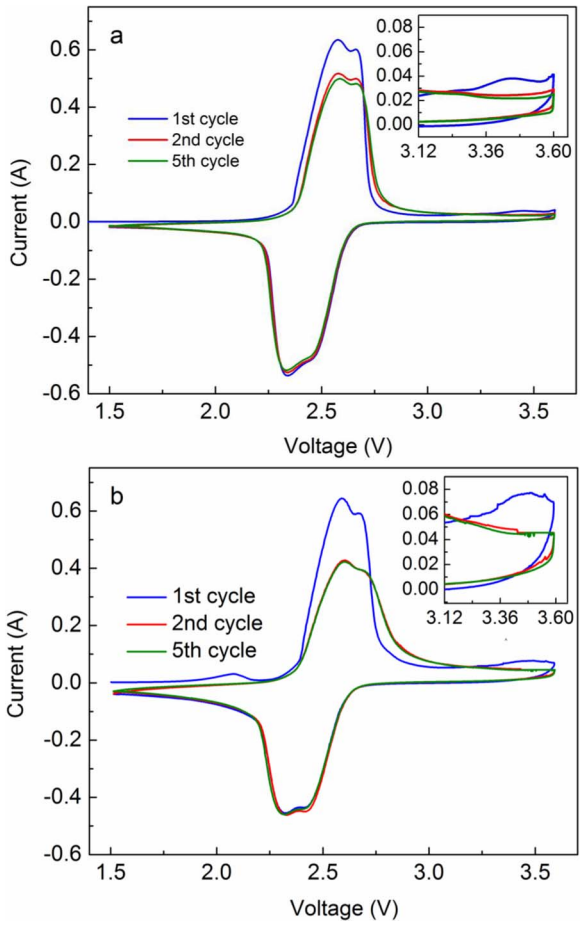

Figure 6. Cyclic voltammograms of (a) $LiMn_2O_4//Li_4Ti_5O_{12}$ and (b) $LiMn_2O_4//Li_4Ti_5O_{12}$/C batteries at a scanning rate of 0.2 mV s^{-1}.

intercalation and de-intercalation processes of lithium ions in the 8a tetrahedral sites of spinel $LiMn_2O_4$.[29,30]

Besides these reversible peaks, we can find different electrochemical reaction peaks during the first and subsequent cycles at about 2.0 and 3.4 V region of $LiMn_2O_4//Li_4Ti_5O_{12}$ and $LiMn_2O_4//Li_4Ti_5O_{12}$/C batteries.

1) In the first cycle, as shown in Fig. 6b, peaks at about 2.1 V may ascribe to the intercalation processes of lithium ions in the pitch derived pyrolytic carbon in $Li_4Ti_5O_{12}$/C. While for $LiMn_2O_4//Li_4Ti_5O_{12}$, it does not have similar peaks.
2) The oxidation peaks (inset of Fig. 6a and 6b) between 3.2 and 3.6 V is due to the electrolyte decomposition reaction, and resulted in the solid electrolyte interphase (SEI) formation on the surface of $Li_4Ti_5O_{12}$ or $Li_4Ti_5O_{12}$/C surface. As shown in Fig. 6a ($LiMn_2O_4//Li_4Ti_5O_{12}$ batteries), decomposition peaks still exist in the 10th cycle of the battery, which means the lack of a protective layer on the surface of $Li_4Ti_5O_{12}$ and continuous electrolyte decomposition. In addition, the decomposed gases, such as hydrocarbon gases and CO are generated in the batteries, resulted in the swelling of the batteries.
3) In contrast to the $LiMn_2O_4//Li_4Ti_5O_{12}$ batteries, the cathodic peaks between 3.2 and 3.6 V for $LiMn_2O_4//Li_4Ti_5O_{12}$/C disappeared (Fig. 6b) after the initial cycles, which proves that the electrolyte decomposition ceased.

$LiMn_2O_4$ and $Li_4Ti_5O_{12}$ have flat operating voltage plateaus of ~4.0 and ~1.5 V, respectively. In the present study, as shown in Fig. 7, the battery capacity was determined by the $Li_4Ti_5O_{12}$ anode (that is, excess $LiMn_2O_4$ cathode material was used to design the battery

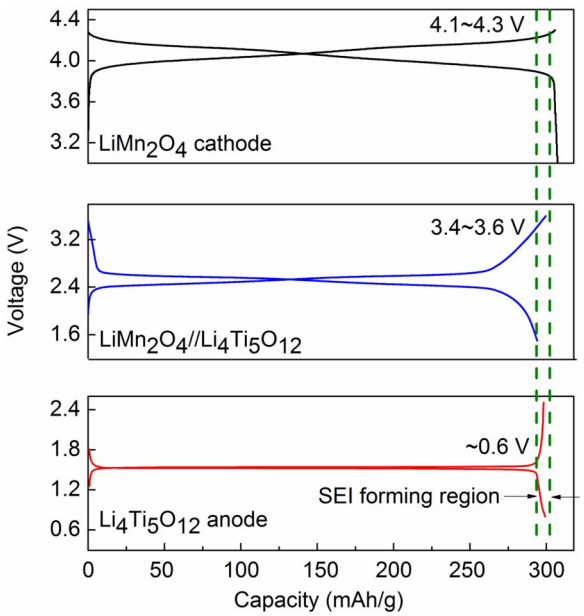

Figure 7. Schematic of battery design for $LiMn_2O_4//Li_4Ti_5O_{12}$ batteries with excess $LiMn_2O_4$ used.

and capacity ratio of $LiMn_2O_4/Li_4Ti_5O_{12}$ is ~1.05). Thus, for this excess cathode designed batteries, at the upper limit of 3.6 V cut-off voltage, the potential of $LiMn_2O_4$ cathode still remains at ~4.1–4.3 V versus Li/Li^+, while the voltage of the $Li_4Ti_5O_{12}$ down to 0.4–0.8V. The voltage window between 0.4 and 0.8V corresponds to the SEI forming region of the anode materials, which is shown in Fig. 7. This design can prevent the overcharge of the cathode material and severe capacity fading for $LiMn_2O_4//Li_4Ti_5O_{12}$ battery systems.[31]

Although excess $LiMn_2O_4$ paired with $Li_4Ti_5O_{12}$ can prevent the overcharge of $LiMn_2O_4$, the lower voltage of $Li_4Ti_5O_{12}$ anode results in the reduction of electrolytes at the electrode surface during subsequent cycling (Fig. 6a and 6b). It is well known that SEI is an essential prerequisite for proper electrode performance in LIBs. For the conventional graphite anode, reduction of electrolyte results in the formation of SEI, which prevents further side reactions during cycling. Unlike graphite anode materials, dense and uniform SEI film does not form on the surface of $Li_4Ti_5O_{12}$ materials, which does not prevent continuous electrolyte decomposition on the catalytic active sites. While for $Li_4Ti_5O_{12}$/C materials, SEI formed on the surface of coated carbon are believed to have homogeneous structure, mechanical flexibility, and strong adhesion to the carbon surface.[32] Therefore, the electrolyte decomposition ceased, as shown in Fig. 6b, and the gas forming reaction can be effectively suppressed by the SEI forming on the carbon layer of $Li_4Ti_5O_{12}$/C materials.

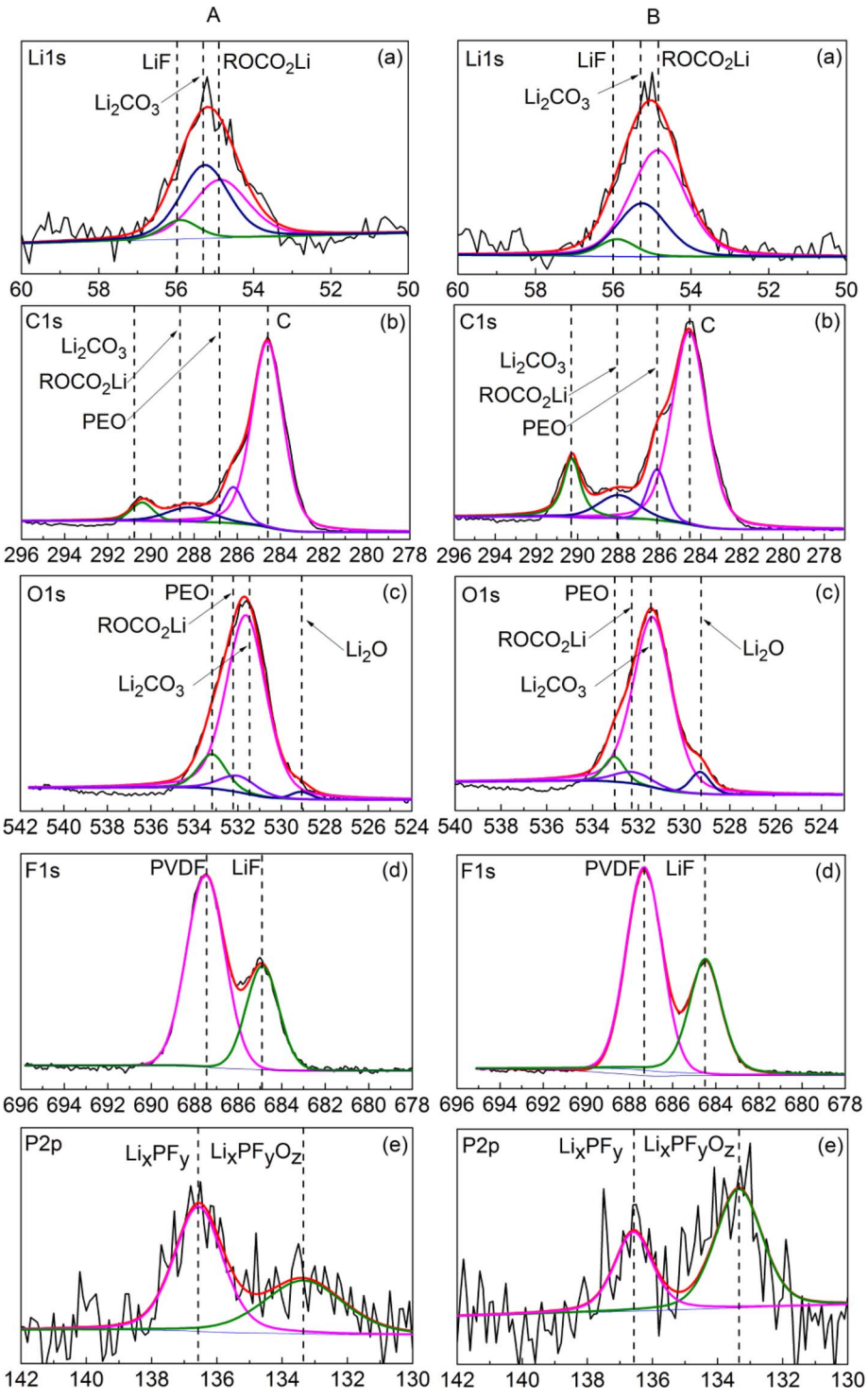

Figure 8. XPS spectra of (A) $Li_4Ti_5O_{12}$ and (B) $Li_4Ti_5O_{12}$/C after 10 cycles at 0% SOC in $LiMn_2O_4$ battery system. (a) Li 1s, (b) C 1s, (c) O 1s, (d) F 1s and (e) P2p.

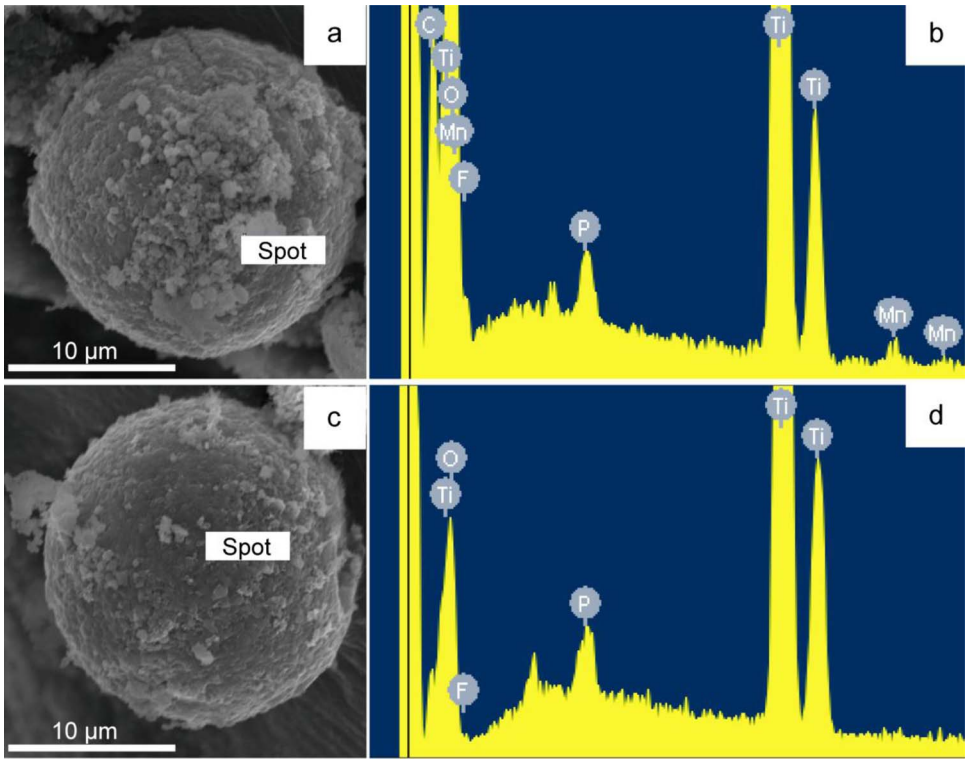

Figure 9. SEM morphologies and energy-dispersive X-ray analysis (EDS) analyses of cycled $Li_4Ti_5O_{12}$ and $Li_4Ti_5O_{12}$/C after 300 cycles at 0% SOC.(a) and (b), $Li_4Ti_5O_{12}$; (c) and (d) $Li_4Ti_5O_{12}$/C.

XPS analysis.— XPS measurements were carried on pouch cells after 10 cycles of charge-discharge. XPS spectra (Fig. 8) for the Li1s, C 1s, O 1s and F 1s shows that LiF, Li_2CO_3, polyethylene oxide (PEO), and $ROCO_2Li$ dominate the main compositions of the SEI film on the surface of $Li_4Ti_5O_{12}$ and $Li_4Ti_5O_{12}$/C materials. Furthermore, the following important points are obtained:

1) In the C1s spectra, the $Li_4Ti_5O_{12}$/C electrode shows more prominent shoulder peaks of carbonates (i.e., Li_2CO_3 at 290.6 eV, $ROCO_2Li$ at 288.6 eV,and PEO at 286.0 eV) than the $Li_4Ti_5O_{12}$ electrode. According to Novak et al.,[32] PEO is usually present in the outermost layer of the SEI close to the electrolyte phase. PEO in the C1s spectra imparts flexibility of the SEI and can further protect the surface of the $Li_4Ti_5O_{12}$ materials during long-time cycling.[32]
2) Comparing O 1s spectra with Li 1s and F 1s spectra, a small peak of Li_2O (529.0 eV) was observed from the SEI film on the surface of $Li_4Ti_5O_{12}$/C electrode, which is more pronounced than that of $Li_4Ti_5O_{12}$.
3) This indicates that the amounts of LiF are more pronounced for $Li_4Ti_5O_{12}$/C than that of $Li_4Ti_5O_{12}$ materials, as shown in F 1s spectra.
4) According to Davidson et al.,[33,34] the P2p spectra generally consists of two main peaks of Li_xPF_y (136.5 eV) and $Li_xPF_yO_z$ (133.4 eV). It can be seen from the P2p spectra that $Li_xPF_yO_z$-rich peak appears on the $Li_4Ti_5O_{12}$/C which is much higher than that of $Li_4Ti_5O_{12}$ electrode materials.

All of these results suggest that carbon can increase the flexibility, uniformity, and amount of the SEI film. Pure $Li_4Ti_5O_{12}$ may have severe side reactions during cycling. According to He and Kang et al.,[23] gassing is due to interfacial reactions between $Li_4Ti_5O_{12}$ and surrounding alkyl carbonate solvents. Gassing even occurs when $Li_4Ti_5O_{12}$ is simply soaked in electrolyte solution (not undergoes any electrochemical process). When carbon is coating, a successive SEI film can be formed on the carbon coating layer of the $Li_4Ti_5O_{12}$/C particles. This uniform SEI can separate the $Li_4Ti_5O_{12}$ from the surrounding electrolyte and can inhibit continuous electrolyte decomposition and gas generation.

Due to effective SEI layer on the carbon coating layer, cycled $Li_4Ti_5O_{12}$ and $Li_4Ti_5O_{12}$/C anode has obvious difference. Figure 9 shows SEM and EDS spectra of the $Li_4Ti_5O_{12}$ and $Li_4Ti_5O_{12}$/C electrode surface after 300 cycles. Clearly, for the $Li_4Ti_5O_{12}$ materials in Fig. 9a, many large porous particles (several micrometers in diameter) dispersed on the surface after cycling. While for the $Li_4Ti_5O_{12}$/C in Fig. 9c, cycled electrode kept spherical morphology. As shown in Fig. 9b, these white particles contained large amounts of Mn. This indicates severe deposition of Mn on the surface of $Li_4Ti_5O_{12}$ samples. Although $Li_4Ti_5O_{12}$/C still has some small white particles, Mn signal of these particles are still undetectable, as shown in Fig. 9d.

In order to confirm the results, we conducted XPS analysis. Mn deposition can also be confirmed by XPS Mn2p spectra of cycled $Li_4Ti_5O_{12}$ and $Li_4Ti_5O_{12}$/C anode materials, as shown in Fig. 10.

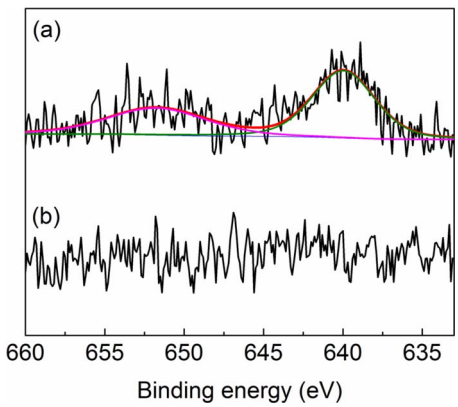

Figure 10. XPS Mn2p spectra of cycled $Li_4Ti_5O_{12}$ and $Li_4Ti_5O_{12}$/C after 300 cycles at 0% SOC. (a) $Li_4Ti_5O_{12}$ and (b) $Li_4Ti_5O_{12}$/C.

In the case of using $LiPF_6$ as the electrolyte salt, $LiPF_6$ can easily react with water, which unavoidably exists in a very low concentration (ppm) in the electrolyte, as shown in the following reaction equations[35,36]

$$LiPF_6 + H_2O \rightarrow POF_3 + LiF + 2HF \quad [1]$$

$$POF_3 + H_2O \rightarrow PO_2F_2^- + HF \quad [2]$$

$$PO_2F_2^- + H_2O \rightarrow PO_3F_2^- + HF \quad [3]$$

$$PO_3F^{2-} + H_2O \rightarrow PO_4^{3-} + HF \quad [4]$$

$LiPF_6$ salt itself also undergoes decomposition during reduction in the charge/discharge cycles, the reactions are as follows

$$LiPF_6 \rightarrow LiF + PF_5 \quad [5]$$

$$PF_5 + H_2O \rightarrow POF_3 + 2HF \quad [6]$$

Decomposition by-products such as HF can attack $LiMn_2O_4$ to yield soluble Mn (II) species, and manganese ionic species will be reduced on the anode surface easily.[37] On the other hand, deposited manganese can effectively catalyze the electrolyte decomposition, which in turn leads to more Mn deposition and gassing.[35,36] This means Mn depositon and electrolyte decomposition (gassing) are highly interrelated and mutually reinforcing.

When carbon is coated on $Li_4Ti_5O_{12}$, a uniform and effective SEI layer formed on the surface of $Li_4Ti_5O_{12}$, and the SEI layer may inhibit continuous electrolyte decomposition. Thus, gassing, Mn decomposition and electrolyte decomposition are ceased together, and Mn deposition is undetectable.

In summary, dual functions of carbon in $Li_4Ti_5O_{12}$/C are as follows: (1) Carbon coating can significantly improve rate capability and cycling performance compared with that of $Li_4Ti_5O_{12}$ materials, (2) Compact and dense SEI protection film can be formed on the surface of the carbon coating layer and inhibit the continuous electrolyte decomposition during cycling, which results in less gassing during cycling.

Conclusions

Coated carbon in $Li_4Ti_5O_{12}$/C microsphere materials play dual functions. Carbon significantly improves the rate capability and cycling performance of $Li_4Ti_5O_{12}$/C materials in $LiMn_2O_4$//$Li_4Ti_5O_{12}$ battery systems. More importantly, the uniform carbon on the surface of $Li_4Ti_5O_{12}$/C microspheres can effectively inhibit Mn deposition on the anode electrode in $LiMn_2O_4$//$Li_4Ti_5O_{12}$ battery systems, which in turn prevents the electrolyte from further reduction decomposition, thus efficiently suppress gassing during charge/discharge processes. The stable interface and excellent electrochemical performance makes $Li_4Ti_5O_{12}$/C microspheres a very promising anode material for large scale LIBs and this simple preparation method enables its production on industrial scale.

Acknowledgments

This work was supported by Ministry of Science and Technology of China (No. 2014CB932402), National Natural Science Foundation of China (No. 51221264 and 51172242), Special Funds for the Development of Strategic Emerging Industries in Shenzhen (No. CXZZ20120824140745535).

References

1. E. Ferg, R. J. Gummow, A. Dekock, and M. M. Thackeray, *J. Electrochem. Soc.*, **141**, L147 (1994).
2. M. M. Thackeray, *J. Electrochem. Soc.*, **142**, 2558 (1995).
3. K. S. Park, A. Benayad, D. J. Kang, and S. G. Doo, *J. Am. Chem. Soc.*, **130**, 14930 (2008).
4. B. H. Li, C. P. Han, Y. B. He, C. Yang, H. D. Du, Q. H. Yang, and F. Y. Kang, *Energy & Environmental Science*, **5**, 9595 (2012).
5. A. S. Prakash, P. Manikandan, K. Ramesha, M. Sathiya, J. M. Tarascon, and A. K. Shukla, *Chem. Mater.*, **22**, 2857 (2010).
6. M. M. Rahman, J. Z. Wang, M. F. Hassan, S. L. Chou, D. Wexler, and H. K. Liu, *J. Power Sources*, **195**, 4297 (2010).
7. M. W. Raja, S. Mahanty, M. Kundu, and R. N. Basu, *J. Alloy. Compd.*, **468**, 258 (2009).
8. H. W. Lu, W. Zeng, Y. S. Li, and Z. W. Fu, *J. Power Sources*, **164**, 874 (2007).
9. E. M. Sorensen, S. J. Barry, H. K. Jung, J. R. Rondinelli, J. T. Vaughey, and K. R. Poeppelmeier, *Chem. Mater.*, **18**, 482 (2006).
10. Y. F. Tang, L. Yang, Z. Qiu, and J. S. Huang, *Electrochem. Commun.*, **10**, 1513 (2008).
11. Y. F. Tang, L. Yang, Z. Qiu, and J. S. Huang, *J. Mater. Chem.*, **19**, 5980 (2009).
12. L. Cheng, X. L. Li, H. J. Liu, H. M. Xiong, P. W. Zhang, and Y. Y. Xia, *J. Electrochem. Soc.*, **154**, A692 (2007).
13. L. Cheng, J. Yan, G. N. Zhu, J. Y. Luo, C. X. Wang, and Y. Y. Xia, *J. Mater. Chem.*, **20**, 595 (2010).
14. R. Dominko, M. Gaberscek, A. Bele, D. Mihailovic, and J. Jamnik, *J. Eur. Ceram. Soc.*, **27**, 909 (2007).
15. D. Capsoni, M. Bini, V. Massarotti, P. Mustarelli, S. Ferrari, G. Chiodelli, M. C. Mozzati, and P. Galinetto, *J. Phys. Chem. C*, **113**, 19664 (2009).
16. D. Capsoni, M. Bini, V. Massarotti, P. Mustarelli, G. Chiodelli, C. B. Azzoni, M. C. Mozzati, L. Linati, and S. Ferrari, *Chem. Mater.*, **20**, 4291 (2008).
17. M. Nakayama, Y. Ishida, H. Ikuta, and M. Wakihara, *Solid State Ionics*, **117**, 265 (1999).
18. J. Gao, C. Y. Jiang, and C. R. Wan, *J. Electrochem. Soc.*, **157**, K39 (2010).
19. S. H. Huang, Z. Y. Wen, J. C. Zhang, Z. H. Gu, and X. H. Xu, *Solid State Ionics*, **177**, 851 (2006).
20. S. H. Huang, Z. Y. Wen, X. J. Zhu, and X. L. Yang, *J. Electrochem. Soc.*, **152**, A1301 (2005).
21. I. Belharouak, G. M. Koenig, T. Tan, H. Yumoto, N. Ota, and K. Amine, *J. Electrochem. Soc.*, **159**, A1165 (2012).
22. Y. B. He, F. Ning, B. H. Li, Q. S. Song, W. Lv, H. D. Du, D. Y. Zhai, F. Y. Su, Q. H. Yang, and F. Y. Kang, *J. Power Sources*, **202**, 253 (2012).
23. Y. B. He, B. H. Li, M. Liu, C. Zhang, W. Lv, C. Yang, J. Li, H. D. Du, B. Zhang, Q. H. Yang, J. K. Kim, and F. Y. Kang, *Sci. Rep.*, **2** (2012).
24. X. Lu, L. Zhao, X. Q. He, R. J. Xiao, L. Gu, Y. S. Hu, H. Li, Z. X. Wang, X. F. Duan, L. Q. Chen, J. Maier, and Y. Ikuhara, *Adv. Mater.*, **24**, 3233 (2012).
25. K. Wu, J. Yang, Y. Zhang, C. Y. Wang, and D. Y. Wang, *J. Appl. Electrochem.*, **42**, 989 (2012).
26. G. Q. Liu, L. Wen, G. Y. Liu, Q. Y. Wu, H. Z. Luo, B. Y. Ma, and Y. W. Tian, *J. Alloy. Compd.*, **509**, 6427 (2011).
27. G. Q. Liu, L. Wen, G. Y. Liu, H. Z. Luo, B. Y. Ma, Q. Y. Wu, and Y. W. Tian, *Metals and Materials International*, **17**, 661 (2011).
28. W. Jiao, N. Li, L. Wang, L. Wen, F. Li, G. Liu, and H. M. Cheng, *Chem. Commun.*, **49**, 3461 (2013).
29. M. M. Thackeray, P. J. Johnson, L. A. Depicciotto, P. G. Bruce, and J. B. Goodenough, *Mater. Res. Bull.*, **19**, 179 (1984).
30. Y. Y. Xia and M. Yoshio, *J. Electrochem. Soc.*, **143**, 825 (1996).
31. H. F. Xiang, X. Zhang, Q. Y. Jin, C. P. Zhang, C. H. Chen, and X. W. Ge, *J. Power Sources*, **183**, 355 (2008).
32. P. Verma, P. Maire, and P. Novak, *Electrochim. Acta*, **55**, 6332 (2010).
33. H. Duncan, Y. Abu-Lebdeh, and I. J. Davidson, *J. Electrochem. Soc.*, **157**, A528 (2010).
34. H. Duncan, D. Duguay, Y. Abu-Lebdeh, and I. J. Davidson, *J. Electrochem. Soc.*, **158**, A537 (2011).
35. L. Yang, M. Takahashi, and B. F. Wang, *Electrochim. Acta*, **51**, 3228 (2006).
36. G. G. Amatucci, A. Blyr, C. Sigala, P. Alfonse, and J. M. Tarascon, *Solid State Ionics*, **104**, 13 (1997).
37. S. Komaba, N. Kumagai, and Y. Kataoka, *Electrochim. Acta*, **47**, 1229 (2002).